Preparation of 2D g-C_3N_4/TiO_2 Heterojunction Nanocomposites for Photocatalytic Applications

Pelin Gündoğmuş[1], Asmae Bouziani[1], Nursev Erdoğan[2], Jongee Park[3], Abdullah Öztürk[1]

[1]Middle East Technical University, Department of Metallurgical and Materials Engineering, 06800, Ankara, Turkey
[2]Advanced Material, Process and Energy Technology Center, Turkish Aerospace Industry, Ankara 06980, Turkey
[3]Atılım University, Faculty of Engineering, Department of Metallurgical and Materials Engineering, 06836, Ankara, Turkey

Abstract

In the present study, 2-dimensional (2D) graphite carbon nitride (g-C_3N_4)/titanium dioxide (TiO_2) nanocomposites have been synthesized to enhance visible light photocatalytic activity of TiO_2. Synthesis of nanocomposites was done in 2 steps. First, g-C_3N_4 was realized by heating the melamine (2,4,6- Triamino-1,3,5-triazine) in nitrogen atmosphere. Then, g-C_3N_4 powder was dissolved in deionized water. Titanium precursor (Titanium tetra isopropoxide) and nitrogen source (HNO_3) were mixed and added into g-C_3N_4 solution in various weight ratios to get g-C_3N_4/TiO_2 nanocomposites of different mass ratios. The microstructural characteristics of the nano composites were examined using X-Ray Diffraction (XRD) and Field Emission Scanning Electron Microscope (FESEM) characterization techniques. After synthesis and characterization, photocatalytic activity of the nanocomposites were measured by methylene blue degradation test under UV light source using UV-Vis spectrophotometer. Results revealed that the composites synthesized had comparable photocatalytic activity with a commercially available well known TiO_2 nanopowder, Degussa P25.

1. Introduction

Metal oxide semiconductor photocatalysts have an important impact for the industrial applications such as environmental remediation, waste water treatment, gas sensors, and solar cell [1,2]. Among the photocatalysts, titanium dioxide (TiO_2) has received great attention due to its easy fabrication and production, high efficiency, abundance, non-toxicity, chemical and biological stability, and low cost [3,4]. However due to the large band gap (2.96, 3.0, and 3.2 eV for brookite, rutile, and anatase, respectively), TiO_2 utilizes only small portion (~5%) of daylight [5]. In order to enhance visible light activity, several strategies including coupling, metal and nonmetal doping, dye sensitization and formation of heterostructures have been tried [6]. Tang et al. stated that formation of heterojunctions between two semiconductors is one of the most efficient method [7].

Graphitic carbon nitride (g-C_3N_4) has lower band gap (2.7 eV) than TiO_2. It provides high stability and easy production but, photocatalytic activity of g-C_3N_4 is limited due to fast recombination rate of electron hole pairs [8,9]. Recently, several researchers have recognized that production of g-C_3N_4/TiO_2 heterojunction composites show better photocatalytic activity than either phase pure TiO_2 or g-C_3N_4 [7,9]. Nonetheless, uncertainty still exists and more research is needed to explore the significance of g-C_3N_4/TiO_2 heterojunction composites for photocatalytic applications.

The purpose of this study was to synthesize the g-C_3N_4/TiO_2 heterojunction composites by hydrothermal process in order to enhance visible light photocatalytic activity of TiO_2 powder. Three g-C_3N_4/TiO_2 nanocomposites of different weight percentages of the constituents were synthesized.

2. Experimental Procedure

2.1. Preparation of g-C_3N_4/TiO_2 composites

The g-C_3N_4 powders were synthesized by heating melamine powder (2,4,6-Triamino-1,3,5-triazine, Aldrich, 99%) at 550 °C for 4 h and cooling to ambient temperature. The heating and cooling rates were 5 °C/min^{-1}. The resultant yellow product (g-C_3N_4) was ground to powder form by using mortar with pestle, and then collected. Next, necessary amount of g-C_3N_4 powder was dissolved in 118 mL deionized water with sonication for 1 h. After that, 8.33 mL nitric acid (HNO_3, Aldrich 70%), used as a catalyzer, was added into the suspension. Later, 6.67 mL Titanium tetra-isopropoxide (TTIP, Aldrich 97%), used for TiO_2 precursor, was added to the mixture dropwise while continuous magnetic stirring for 30 min. When dissolution of the TTIP was complete, the solution was transferred into the Teflon-lined autoclave for commencing the hydrothermal reaction(s). Hydrothermal process took place at 110°C for 1 h. At the end of 1 h, resultant g-C_3N_4/TiO_2 nanocomposite was

washed with distilled water for several times until the pH becomes neutral, centrifuged, dried at 80 °C for 24 h, and grounded to powder.

The g-C_3N_4/TiO_2 nanocomposites synthesized were named according to the g-C_3N_4 percentage as TCN-40, TCN-60, and TCN-80 which contained 40, 60, and 80 wt% g-C_3N_4, respectively.

2.2. Characterization of g-C_3N_4/TiO_2 composites

The phases present in the g-C_3N_4/TiO_2 nanocomposites synthesized were identified using an X-ray diffractometer (Rigaku, D/MAK/B, Tokyo, Japan). A scanning rate of 2º/min was applied between 20 to 60º for all samples. The size, shape, and morphology of the nanocomposites were examined by field emission scanning electron microscope (FESEM, Nova, Nanosem) at a voltage of 18 kV. Before the FESEM analysis, all samples were coated with gold using gold sputter to get the desired conductivity.

2.3. Photocatalytic Measurement

The photocatalytic activity of the nanocomposites synthesized was measured by Methylene Blue (MB) degradation test under a 125 W UV lamp with a wavelength at 365 nm and continuous stirring using a magnetic stirrer. The MB solution was prepared first by dissolving 20 mg of MB in distilled water to get a concentration of 20 mg/L and then adding TiO_2 nanoparticles to this solution under continuous stirring to get the TiO_2/MB concentration of 100 mg/20 mL. Before illumination of the UV light, the suspension aqueous solution was stirred continuously in dark for 30 min to ensure adsorption/desorption equilibrium.

At the end of first 30 min, a 3.5 mL analytical sample was taken from the suspension via syringe. Then, by means of syringe filters (Millex Millipore, 0.22 µm) a clear, powder free solution of MO is transferred into quartz cuvette for the UV–Vis spectrophotometer (Shimadzu UV-1800) measurement. After the first measurement, the UV lamp was turned on and change in absorbance values under UV light were measured for every 30, 60, and 90 min while keeping the powders in the MB solution. The MB removal efficiency of the photocatalyst was calculated using Eq. 1.

$$\text{Degradation \%} = (C_o - C)/C_o \times 100 \quad (1)$$

where C_o and C are the concentrations of MB at initial and at different irradiation time, respectively. Color change of the MB solution was assessed by the naked eye. Absorption data of the nanocomposites were compared with that of a well-known commercially available TiO_2 powder (P25 Degussa).

3. Results and Discussion

3.1. X-Ray Diffraction (XRD) Analysis

X-ray diffraction patterns of the nanocomposites TCN-80, TCN-60, and TCN-40 as well as phase pure g-C_3N_4 and TiO_2 are demonstrated in Figure 1. In the XRD pattern of the phase pure TiO_2, the characteristic peaks located at 25.4°, 37.6°, 48°, and 54° corresponding to 101, 201, 200, and 105 planes of anatase phase was detected. An XRD peak at 27.6° belonging to (002) plane of g-C_3N_4 was obvious in the pattern of phase pure g-C_3N_4. Additionally, the XRD pattern of g-C_3N_4 indicated the carbon (C) peak for (002) plane due to residual C. Results revealed that heating melamine at 550 °C for 4 h was not sufficient to convert all melamine to g-C_3N_4. All the nanocomposites synthesized (TCN-80, TCN-60, and TCN-40) indicate both the characteristic anatase peaks located at 25.4°, 37.6°, 48°, and 54° and g-C_3N_4 peak located at 27.6°. It is obvious that as TiO_2 content increases, the intensity of the g-C_3N_4 peak decreases gradually while anatase peaks increases sharply. In the XRD pattern of TCN-80 nanocomposite, anatase peak corresponding to (101) plane was absent. However, TCN-60 and TCN-40 nanocomposites exhibited an overlap of C (002) peak and anatase (001) peak.

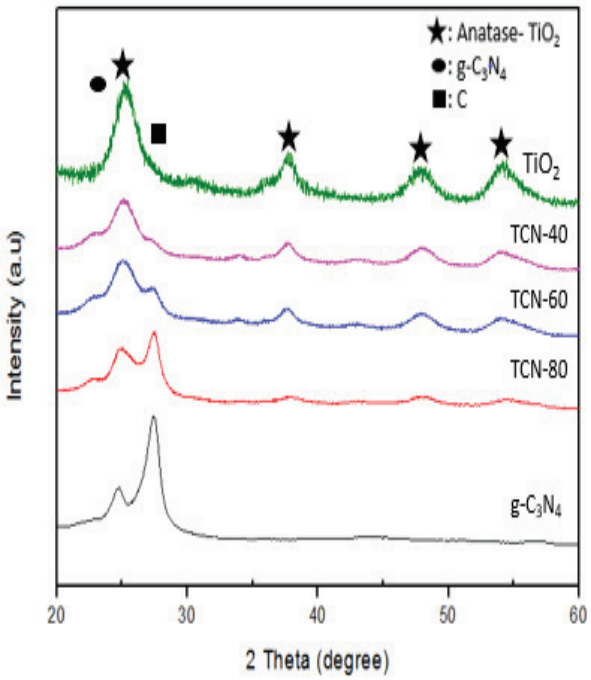

Figure 1.XRD patterns of the nanocomposites TCN-80, TCN-60, and TCN-40, and phase pure g-C_3N_4 and TiO_2.

3.2. SEM Analysis

Figure 2 illustrates representative FESEM images of the synthesized phase pure TiO_2 nanoparticles and g-C_3N_4/TiO_2 heterojunction nanocomposites. It is clearly seen in the image in Figure 2 (a) that phase pure TiO_2 consists of nearly spherical and agglomerated nanoparticles. Size of the nanoparticles is in the range of 10-40 nm and has a uniform distribution. Figure 2 (b) shows the FESEM image of TCN-40 nanocomposite. Due to low g-C_3N_4 content, the microstructure of the nanocomposite did not change much. The microstructure shows that the structure composed of dominantly TiO_2 nanoparticles. Although g-C_3N_4 nanoparticles are present in the structure, they are not detected visibly. Stacked lamellar structure of g-C_3N_4 nanoparticles appear between the spherical TiO_2 nanoparticles as seen in Figure 2 (c). Similar results have been reported by Li et al. [10]. The FESEM image of TCN-80 nanocomposite is shown in Figure 2 (d). TiO_2 nanoparticles grew on the surface of g-C_3N_4 [11]. The increase in g-C_3N_4 content caused an increase in the stacked lamellar structures. TiO_2 nanoparticles occurred on the lamellar structures as agglomerates. When a comparison is made between the FESEM images of the phase pure TiO_2 and all of the g-C_3N_4/TiO_2 nanocomposites, it is noticed that the nanocomposites contain more porosity then phase pure TiO_2. Also, the particle size of the lamellar structure of g-C_3N_4 is bigger than the spherical TiO_2 nanoparticles.

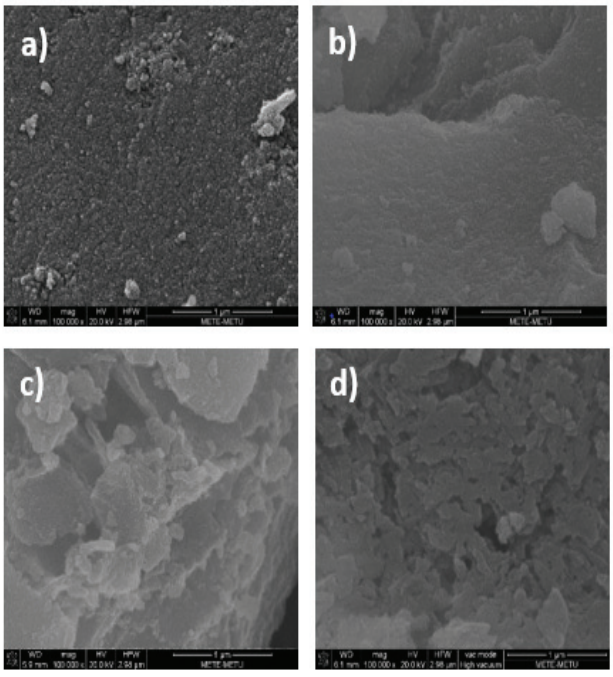

Figure 2. SEM images of (a) phase pure TiO_2, (b) TCN-40, (c) TCN-60, and (d) TCN-80.

3.3. Photocatalytic Activity

Phase pure TiO_2 nanoparticles and the nanocomposites exhibited some degree of photocatalytic activity. Color change of the MB solution was obvious and could be seen easily by the naked eye depending on the composition of the nanocomposites synthesized. Table 1 presents the calculated absorption and degradation data of the TiO_2 nanoparticles.

Table 1: Calculated absorption and degradation data of the TiO_2 nanoparticles.

Absorption (Dark)	Degradation (UV)		
30 min	30 min	60 min	90 min
67.25	40.25	47.55	78.97

The time dependent absorbance spectra of the phase pure TiO_2 nanoparticles in MB solution under UV light are shown in Figure 3. Methylene blue has a higher absorbance than the solutions containing TiO_2 nanoparticles in dark and in UV light at λ=663 nm. Similar results have been reported by Yao and Wang [12]. A remarkable decrease in the absorbance was observed when the MB solutions containing TiO_2 nanoparticles were tested in dark for 30 min. The measurements in dark suggest that the synthesized TiO_2 nanoparticles have high photodegradation ability. When the MB solutions were exposed UV light, the absorbance continued to decrease. The absorbance also decreased when UV illumination time increased from 30 min to 90 min. After 90 min, peak absorbance was very low becauseTiO_2 nanoparticles degraded almost all of the MB molecules that caused to obtain higher photocatalytic activity.

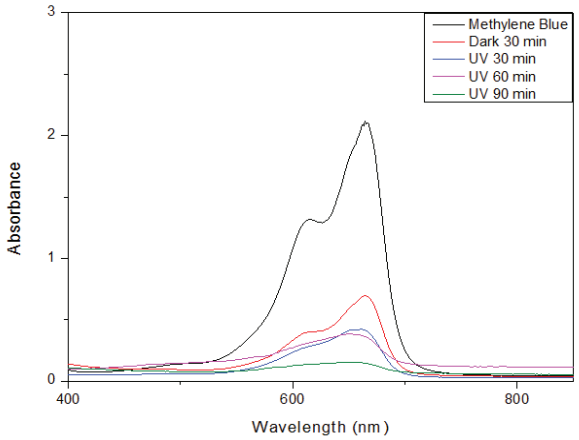

Figure 3. Absorbance versus wavelength spectra of the TiO_2 nanoparticles.

4. Conclusions

1. g-C_3N_4/TiO_2 nanocomposites could be produced by hydrothermal process.

2. TiO_2 nanoparticles deposit on g-C_3N_4 surface in the structure of g-C_3N_4/TiO_2 nanocomposites.

3. The g-C_3N_4/TiO_2 ratio has a profound influence on the microstructure developed in the nanocomposites and on their photocatalytic activity.

4. The photocatalytic activity of TiO_2 nanoparticles could be enhanced by the production of g-C_3N_4/TiO_2 heterojunction composites.

Acknowledgment

The authors would like acknowledge the Scientific and Technological Council of Turkey (TUBITAK) for the partial financial support through project 216M391.

References

[1] N. Erdogan, A. Ozturk and J. Park, Ceramic International, 42 (2016) 5985–5994.
[2] T. Balaganapathi, B. Kaniamuthan, S. Vinoth, T. Arun and P. Thilakan, Ceramic International, 43 (2017) 2438–2440.
[3] E. Asadollahi, A. Youzbashi and M. Keyanpourrad, Journal of Molecular Structure, 1128 (2017) 612–618.
[4] A. Di Paola, M. Bellardita and L. Palmisano, Catalysts, 3 (2013) 36-73.
[5] S. M. Gupta and M. Tripathi, Chinese Science Bulletin, 56 (2011) 1639–1657.
[6] Y. Wang, W. Yang, X. Chen, J. Wang and Y. Zhu, Applied Catalysis B: Environmental, 220 (2018) 337–347.
[7] H. Tang, S. Chang, L. Jiang, G. Tang and W. Liang, Ceramic International, 42 (2016) 18443–18452.
[8] X. Chen, J. Wei, R. Hou, Y. Liang, Z. Xie, Y. Zhu, X. Zhang and H. Wang, Applied Catalysis B: Environmental., 188 (2016) 342–350.
[9] G. Zhang, T. Zhang, B. Li, S. Jiang, X. Zhang, L. Hai, X. Chen and W. Wu, Applied Surface Science, 433 (2018) 963–974.
[10] C. Li, Z. Sun, Y. Xue, G. Yao and S. Zheng, Advanced Powder Technology, 27 (2016) 330–337.
[11] Z. Li, G. Jiang, Z. Zhang, Y. Wu and Y. Han, Journal of Molecular Catalysis A: Chemistry, 425 (2016) 340–348.
[12] J. Yao and C. Wang, International Journal of Photoenergy, 2010 (2010) 1-6.